Extrinsic controls on turbidity fan lobes spatial distribution and potential reservoir presence prediction in half-graben lacustrine basin during early syn-rift: insights from stratigraphic forward modelling

Bingyi Chen[1,2], Peter M. Burgess[2], Chengyan Lin[1*], Lihua Ren[1*], Chunmei Dong[1], Zheng Cao[3]

1. School of Geosciences, China University of Petroleum (East China), Qingdao, China, 266580;

2. Quantitative Experimental Stratigraphy Group, Jane Herdman Laboratory, Department of Earth, Ocean, and Ecological Science, University of Liverpool, Brownlow Street, Liverpool, L69 3GP, United Kingdom

3. School of Petroleum Engineering, Chongqing University of Science and technology, Chongqing, 401331, China

Abstract

Turbidite strata are common along faulted margins of half-graben lacustrine basins, but complex lobe evolution may cause significant variability and uncertainty in the spatial distribution of turbidite sand bodies. This study integrates core samples, seismic and well log data from the Dongying Depression lacustrine basin in East China, and uses these data as inputs to a reduced-complexity stratigraphic forward model of turbidite fan lobe evolution. Data-unconstrained sensitivity analysis is used to investigate sensitivity of fan-lobe spatial distribution to fault-related subsidence rate, basin-margin slope, sediment input volume, and sediment input volume oscillation period. A data-constrained multiple-scenario approach then varied parameters within defined uncertainty ranges to generate a series of best-fit models to predict optimal reservoir presence locations. Results indicate that syn-rift segmentation of the Shengbei fault leads to spatial and temporal variation of fault-related subsidence in the hanging wall basin. External controls exert systematic impact on the spatial distribution of both smaller-scale flow beds and larger-scale fans on basin floor. Higher rates of fault-related subsidence and smaller sediment input volume produce more laterally confined fan lobe distribution. Higher basin-margin slope gradient produces more laterally clustered turbidites, but does not change fan lobe location, indicating break of slope is a more significant control on fan location. Multiple scenario reservoir presence probability maps suggest that bypass-dominated middle and inner fan areas, and smaller lengths of retrogradation-dominated feeder channels are most promising reservoir locations.

Keywords: Extrinsic controls, turbidity fan lobe, spatial distribution, early syn-rift, stratigraphic forward modelling, reservoir presence

1 Introduction

Ancient lacustrine basins are often prospective for hydrocarbons, providing potentially important energy resources, but also perhaps important reservoirs to sequester carbon.

Lacustrine basin faulted-margins particularly favour occurrence of turbidity flows that form sub-lacustrine fans (Weimer et al., 2000; Qiang et al., 2005; Zhao et al., 2018; Liu & Xiong, 2021; Luan et al., 2022). However, the complex nature and spatial distribution of turbidite fan lobes has been demonstrated in modern sedimentary process, ancient outcrops, subsurface strata, flume experiment (Nelson et al., 2009; Prelat et al., 2009, 2010; Koo et al., 2016; Ferguson et al.,2020) and also some numerical modelling (Groenenberg et al., 2010; Burgess et al., 2019). This complexity influences reservoir properties such as vertical connectivity, sand thickness, and grain size distribution (Sprague et al., 2005; Starek et al., 2017; Cullis et al., 2018), complicating predictions of potential reservoir presence and likely behaviour during injection of CO_2.

To successfully explore for, develop, produce and then reuse these tight oil and gas reservoirs for sequestration, better prediction of the most likely location for optimal reservoir properties is required. Prediction depends on an understanding of fundamental controls on spatial distribution and evolution of turbidite sand bodies (Sprague et al., 2005). Previous studies have revealed that fan lobe dynamics and resultant strata are subject to both extrinsic and intrinsic controls (Cecil, 2003; Sprague et al., 2005; Nelson et al., 2009; Hamilton et al., 2013; Haas et al., 2016; Burgess et al., 2019; Ferguson et al.,2020; Meek et al., 2020). Intrinsic factors such as channel avulsion and incision, channel backfilling, and topographic compensation largely control the architecture of smaller-scale fan lobe deposition on basin floor (Meek et al., 2020, Ferguson et al.,2020), whereas extrinsic factors including tectonics, climate, water-level fluctuation, sediment supply etc. dominant at larger spatial and longer temporal scale (Groenenberg et al., 2010; Meek et al., 2020). Most previous studies emphasised intrinsic processes (Hamilton et al., 2013; Haas et al., 2016; Prelat et al., 2010; Wang et al., 2011; Miller et al., 2014), and influence of extrinsic process is less studied. Moreover, for those studies on extrinsic controls, greater importance is attached to sediment supply and sea or lake-level fluctuation (Normark et al., 2006; Knudson & Hendy, 2009; Ferguson et al.,2020), whereas few of them have investigated the influence of fault-related subsidence and margin slope (Normark et al., 2006; Meek et al., 2020). Therefore, analysing this range of extrinsic controls can provide us with a more comprehensive understanding on the interplay between extrinsic and intrinsic controls, and can also assist the prediction on potential reservoir presence and performance.

Traditionally, reservoir prediction is primarily driven by the data collected from basin including core samples, well logging, seismic data etc. However, relying on these datasets alone can be insufficient to accurately characterize strata given the uncertainties arising from complex geological process (Burgess et al., 2006; Gervais et al., 2017). Numerical stratigraphic forward modelling, however, provides practical and effective solution to address these problems because it can examine the influence of various controlling variables using a multiple-scenario approach to generate conditional probability maps that predict reservoir presence (Burgess et al., 2006; Gervais et al., 2017). A reduced-complexity stratigraphic forward model Lobyte3D is applied in this study in order to achieve the following goals: (1) to investigate both the paleoclimate-related (sediment input volume and sediment input oscillation period) and tectonic-related (fault-related subsidence and margin slope) extrinsic controls on fan lobe lateral movement, to better understand the sensitivity and contribution of these allogenic factors to the turbidity fan lobe spatial distribution in the faulted margin of an Eocene half-graben lacustrine basin, (2) to quantify the uncertainty range of the considered extrinsic parameters, (3) to produce predictive reservoir presence probability maps.

2 Geological setting

Bohai Bay Basin is a Mesozoic-Cenozoic continental rift basin located at East China, which comprises seven tectonically related petroliferous sub-basins (Jiyang, Hunaghua, Jizhong, Linqing, Bozhong, Liaodong Bay and Liaohe) separated by major internal uplifts within the Bohai Bay Basin (Allen et al., 1997) (Fig 1a). The Dongying Depression, a typical fault-controlled extensional lacustrine basin trending in NEE, is located at the southeast of Jiyang sub-basin, extending 90 km in W-E and 65 km in N-S and covering an area of approximately 5700km^2 (Wang et al,2016). Dongying depression is structurally shaped into an asymmetrical, half-graben basin by a faulted steep-slope margin to the north and a hinged gentle-slope margin to the south, surrounded by six major topographic highs raising from Precambrian basement (Chenjiazhuang Rise to the north, Qingtuozi Rise to the east, Binxian Rise to the northwest, Qingcheng Rise to the southwest, Guangrao rise to the southeast, and Luxi Uplift bounding to the south), and could be further segmented into four sags within the depression: Lijin Sag, Minfeng Sag, Boxing Sag, and Niuzhuang Sag (Zhang et al., 2009) (Fig 1b, 1c).

The formation of Dongying depression occurred in three primary stages: Precambrian crystalline basement formation and consolidation platform stabilization from the late Proterozoic to the Paleozoic, and basin-rifting during the Cenozoic (Tao et al., 2022). Cenozoic rifting of the Doingying depression involved Paleogene syn-rift differential subsidence followed by Neogene post-rift thermal subsidence. Paleogene rifting is composed of four rifting episodic stages: (1) pre to early rifting from the Paleocene to the Early Eocene (65–50.4 Ma); (2) early rifting from the Early to the Middle Eocene (50.4–42.5 Ma); (3) rift climax from the Middle to the Late Eocene (42.5–38 Ma); and (4) late rifting from the Late Eocene to the Oligocene (38–24.6 Ma) (Tao et al., 2022; Feng et al., 2013) (Fig 2). Rift faults occur across a range of different scales, mostly oriented W-E and SW-NE (Allen et al., 1997). The Chengnan Fault, active from late Mesozoic to Late Cenozoic, is the N-E trending regional basin boundary fault separating the basin from the Chenjiazhuang Rise in the north. The Shengbei fault sets and other lower-order faults comprise the 'northern faulted margin' in the Dongying depression (Zhang et al., 2009; Tao et al., 2022).

Paleogene strata are underlain by the Mesozoic pre-rift basement and disconformably overlain by post-rift Neogene fluvial strata. Paleogene strata comprise three formations, from bottom to the top the Kongdian (Ek), Shahejie (Es), and Dongying (Ed) formations (Feng et al., 2013). The upper part of the fourth member of Shahejie formation ($Es4^1$) is the main interval of interest in this study. The Shahejie Formation (Es) comprises four members. The fourth member of Shahejie Formation (Es4) was deposited when the Dongying depression lake deepened and expanded due to ongoing rifting. It starts with alternating layers of red sandstone and mudstone, interbedded with salt in its lower part ($Es4^2$)

transitioning to black shale and grey mudstone intercalated with sandstones and thin limestone layers in its upper part ($Es4^1$). It is overlain by the third member of Shahejie formation (Es3) consisting predominantly of oil shale, dark mudstones and interbedded fine-grained sandstones (Allen et al., 1997) from deep lacustrine environment during rift climax stage. The subsequent second member (Es2) and first member(Es1) of Shahejie Formation are deposited in shallow lacustrine during the lake shrinkage period resulting from the attenuation of tectonic activity, both with higher proportion of coarser terrigenous clastic. The Shahejie Formation is comformably overlain by the Dongying formation and mainly comprised of fluvial-deltaic deposits including coarse sandstone, medium-fine sandstones interbedded with greyish to reddish mudstone, marking the end of late-rifting stage (Allen et al., 1997; Feng et al., 2013; Tao et al., 2022) (Fig 2).

The study area is located in the northeast of Lijin sag, a hanging wall basin immediately bounded by the Shengbei fault within the northern faulted margin of the Dongying depression (Fig 1d, 1e). Chenjiazhuang rise to the north was the primary local sediment sources, with the Binxian rise to the west, the Qingtuozi rise to the east, and a central diapiric anticline to the south. The upper part of the fourth member of Shahejie formation ($Es4^1$), which is the interval of interest in this study, were primarily deposited during the early syn-rift stage, with thickness ranging between 800m to 900m and burial depth between 3300m to 4500m. It can be further divided into two parts by a regionally continuous mud layer: ChunX (stage one) and the overlying ChunS (stage two) (Fig 1e). During the deposition of $Es4^1$, the study area was undergoing lake expansion and lake level increase, with superimposed lake-level oscillations (Jiang et al., 2011). The semi-arid to humid climate produced an increasing amount of siliciclastic sediment supply from the up-dip Chenjiazhuang rise, together with intensified tectonic events along Shengbei fault, resulting in numerous turbidites in the study area (Yang et al., 2019). The turbidites are characterised by relatively thin-bedded greyish fine-medium sandstone to sandy gravel interbedded with thick-bedded grey-to-dark mudstone (Fig 3).

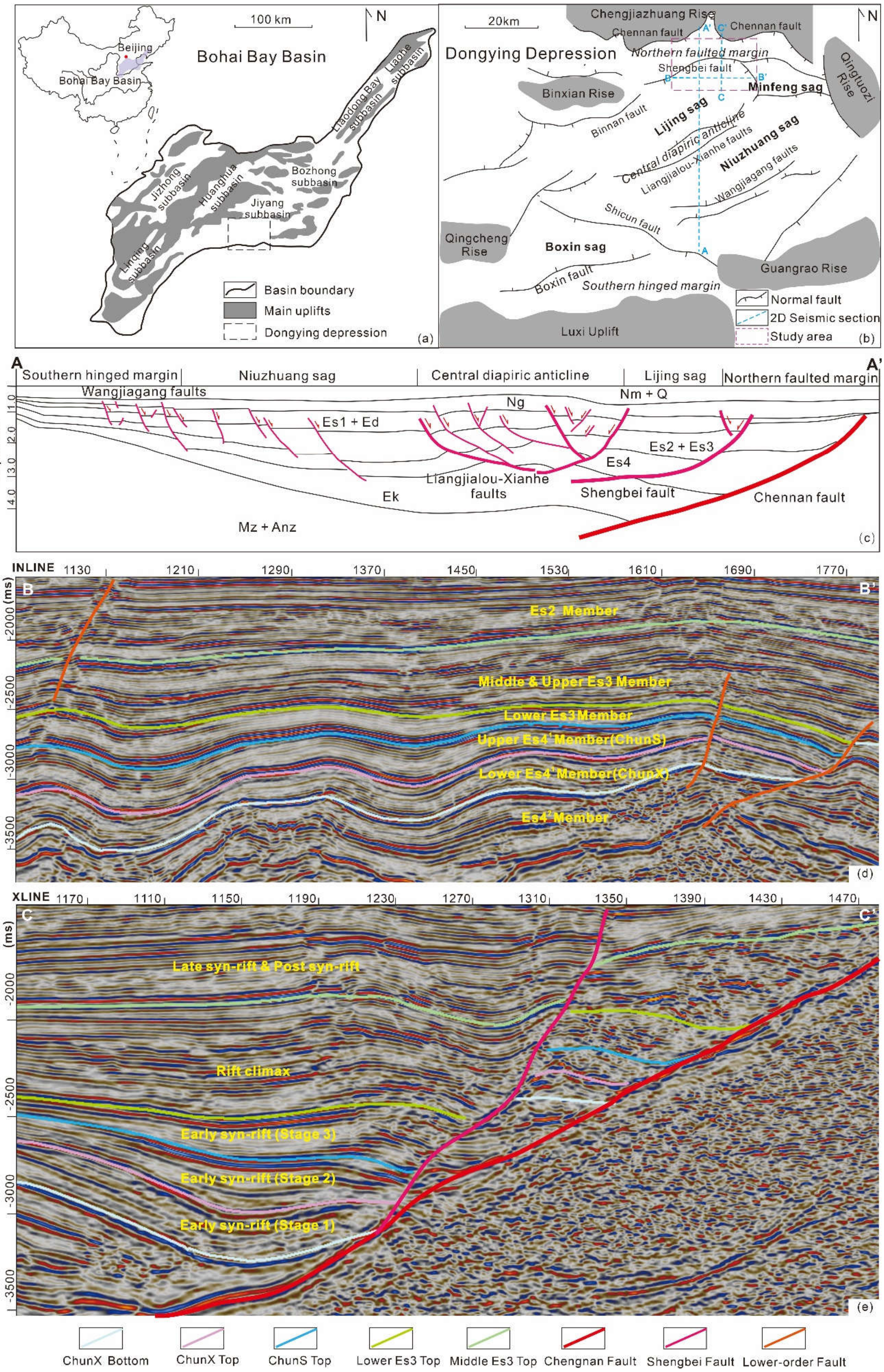

Figure 1: Location map of study area showing (a) the sub-tectonic units of the Bohai Bay Basin and (b) structural features of Dongying depression. (c) N-S tectonostratigraphy section of Dongying depression showing the northern faulted margin and southern hinged margin, (d) W-E seismic section profile B-B' of the

study area. (e) N-S seismic section profile C'-C of the study area

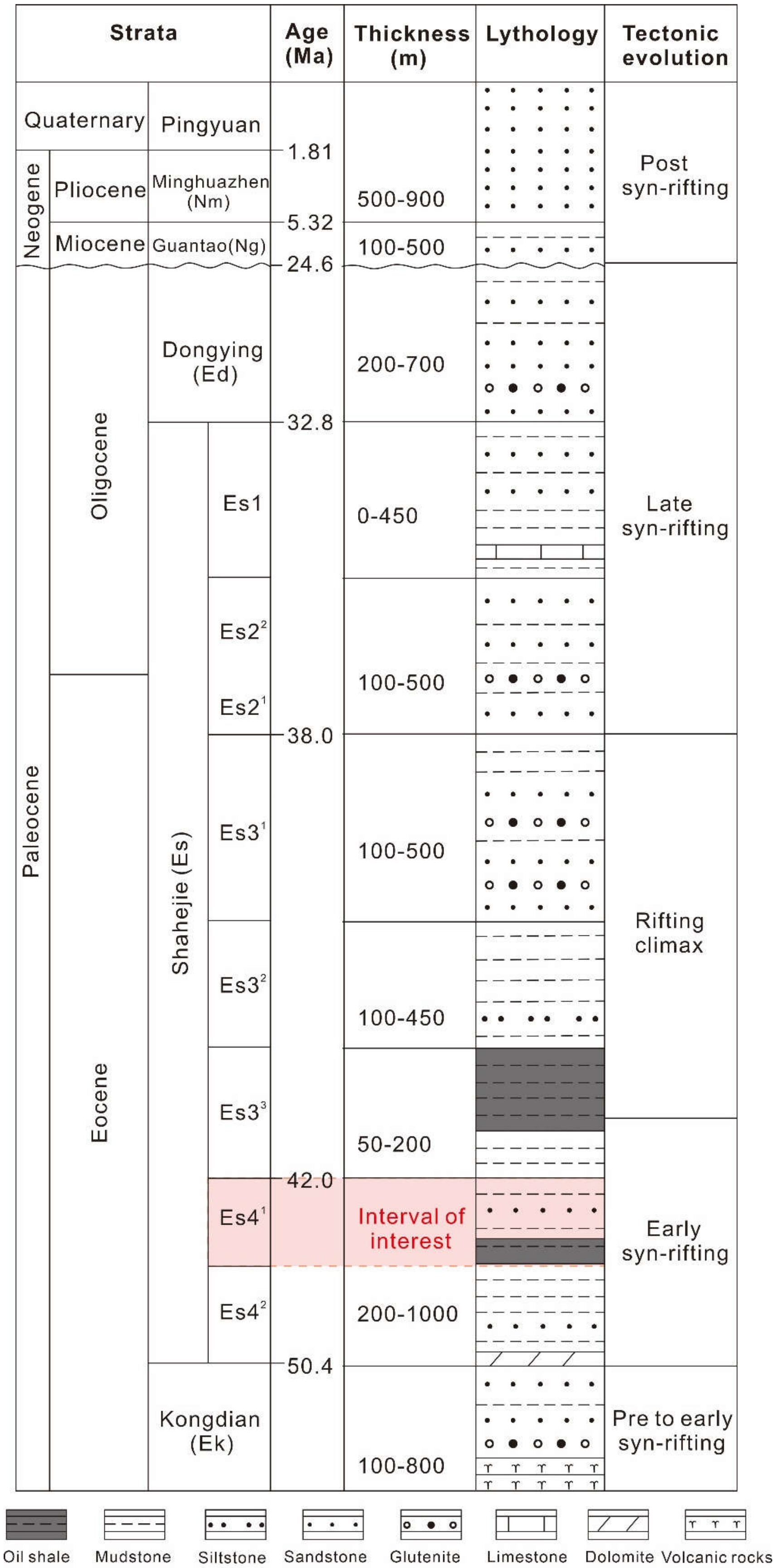

(e)

Figure 2: Summary Stratigraphic column for Cenozoic–Pleistocene strata in the Dongying

depression lacustrine basin.

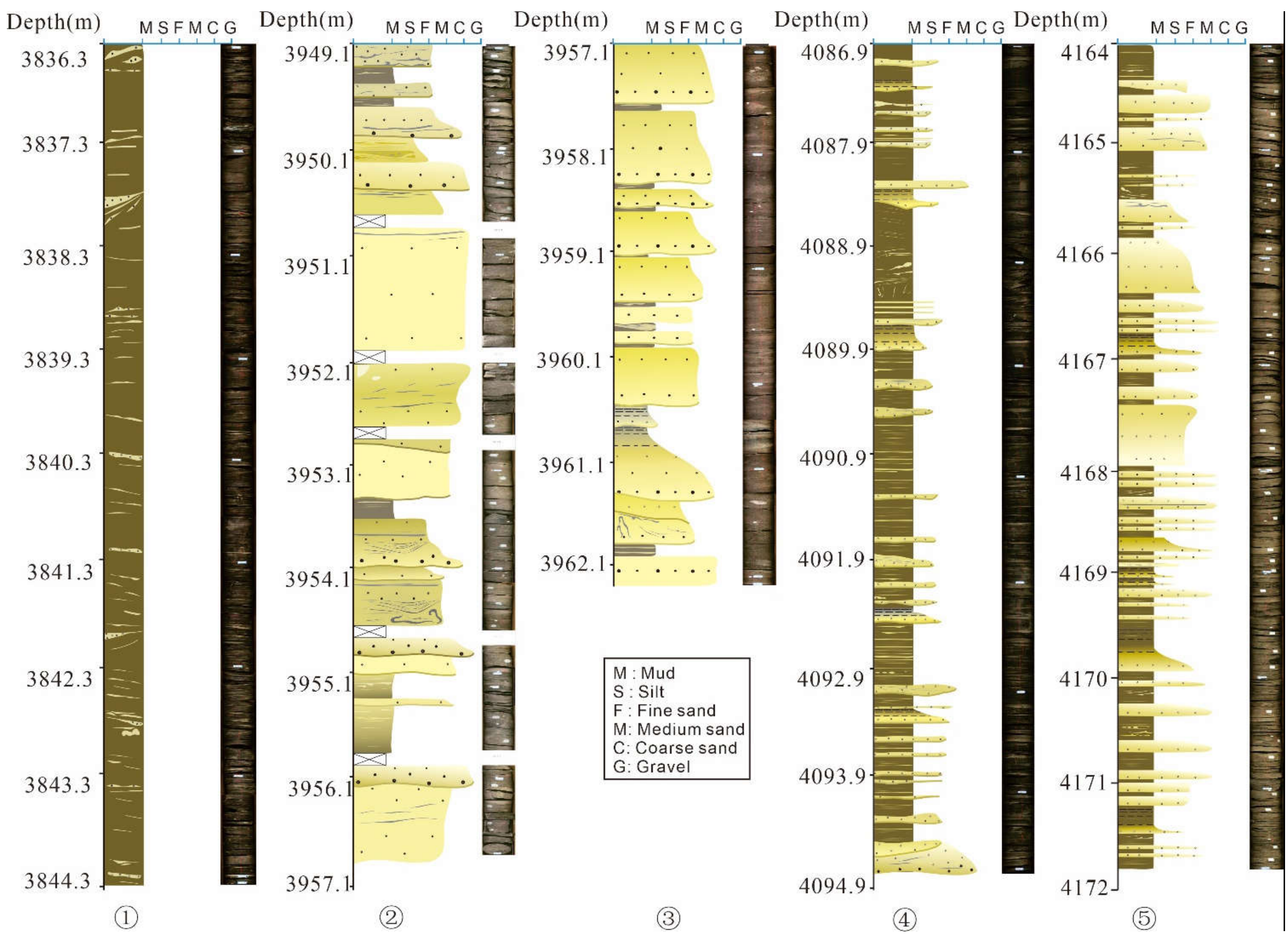

Figure 3: Lithology sketch of core samples from Well 1 in the study area. Thin-bedded greyish fine-medium sandstone to sandy gravel turdidites are interbedded with thick-bedded grey to dark mudstones

3 Data and methods

This study is primarily based on datasets supplied from Shengli Oil Field, China Petroleum & Chemical Corporation (SINOPEC), including 3D seismic data, horizon data, well log data of four wells and scanning photos of cores samples from one well. The 3D seismic data cover an area of 247km^2 (19km*13km), with sampling interval of 1ms and bin spacing of 25m, a frequency range from 10 Hz to 40 Hz, and a dominant frequency at 25 Hz. Conventional well-log data include spontaneous potential, resistivity, natural gamma, acoustic, and density logs.

3.1 seismic and well log interpretation

Seismic interpretation used Schlumberger's Petrel and well log interpretation used ResForm. Based on seismic horizon interpretations, displacement rate along the Shengbei fault during stage one and stage two of $Es4^1$ deposiiton is calculated via 'throw back-stripping' (Dawers et al., 1995; Nixon et al., 2016; Ma et al., 2020; Alghuraybi, 2021) -- using the thickness projection difference (TWT in ms,) between hanging wall and footwall across syn-depositional fault, to reflect the faulting activity variation along fault strike. Additionally, major turbidity fan lobes deposited during ChunX (stage one) and ChunS (stage two) of $Es4^1$

are identified, picked and mapped based on their geometry and termination patterns. A seismic-to-well tie, based on synthetic seismograms, verifies the credibility of fan lobe interpretation from seismic. Fan lobe area and sediment volume are calculated for each interpreted lobe, and cutting logs and core photos allow calculation of the number of individual turbidity events contained in each interpreted fan lobe.

3.2 Stratigraphic forward modelling—Lobyte 3D

A reduced-complexity model Lobyte 3D is used to produce three-dimensional fan strata model, and to test the sensitivity of turbidity fan lateral mobility to multiple external influence in this study. Lobyte 3D consists of a pre-defined number of time-steps, with one turbidity flow events per time step, starting at a single point-source origin, flowing down slope, decelerating as slope decreases and depositing dispersively. There are two primary turbidity current processes included in Lobyte 3D, erosive and bypassing downslope sediment transport generating feeder channels, and dispersive flow deposition producing fan lobes. Fine grained hemiplegic deposition occurring at a fix rate caps the turbidite deposition at each time step (Burgess et al., 2019, Mackie et al. in review).

Sediment supply parameters specify the sediment volume of each flow event. Flows are fed from source points that can be pre-defined at any position on the model grid. Flows are assumed to occupy a single model grid point and follow a steepest gradient downslope. Flow velocity is a function of topographic gradient and flow thickness, calculated with a Chezy-type formula appropriate for low concentration flows under steady, turbulent, open channel flow conditions such that:

$$U = \sqrt{\frac{\rho_g g C_v H_f sin\theta}{C_d}} \quad (1)$$

where ρ_g is the specific density of sediment in water, *g* is gravitational acceleration (9.81m/s^{-2}), C_v is flow sediment concentration (dimensionless), H_f is the height of the velocity maximum from the bed (flow thickness), ϑ is the downstream angle of dip, C_d is basal friction coefficient (dimensionless).

In this reduced-complexity model, a single grain diameter is used for all calculations. This allows particle settling velocity v_s of the modelled grain size to be used as the threshold for sediment transport (Burgess et al., 2019; Mackie et al. in review):

$$v_s = \frac{v}{d50}\left[(10.36^2 + 1.049D_*{}^3)^{1/2} - 10.36\right] \quad (2)$$

Where v = kinematic viscosity of water, d_{50}= median grain size, and D_* the non-dimensional grain size parameter.

If the velocity U is above a calculated threshold, the flow will erode and entrain sediment (E_s) following:

$$E_s = v_s \frac{A\left(Z^{'}\right)^5}{1 + \frac{A}{0.3}\left(Z^{'}\right)^5} \quad (3)$$

where *A* is an empirically derived constant (1.3× 10^{-7}), v_s is particle settling velocity, and $Z^{'}$ is modified tractive stress

Two conditions trigger deposition. If the flow velocity U decreases below the threshold for sediment transport, the flow will begin to deposit its load. The flow velocity U is compared with a deposition threshold velocity U_{depos} to determine whether the flow continues to flow down slope, or starts to deposit. Deposition commences at the point where $U < U_{depos}$. Deposition can also be triggered through interaction with topography. If the flow encounters a topographic obstacle with a height less than flow thickness, the flow will become partially blocked and deposit.

During deposition downslope flow continues and the flow volume flux into each surrounding cell is proportional to topographic slope. Proportion, ΔV_k, of sediment volume $V_{i,j}$ received by each surrounding cell is calculated by:

$$\Delta V_k = \left[{G_k}^{FRF} . \left(\sum_{k=1}^{8} G_k\right)^{-1}\right] . V_{i,j} \quad where\ k = 1,2,3, \dots ,8; \qquad (4)$$

where G_k is the gradient form the source cell, FRF is flow radiation factor which controls the degree of flow dispersion (Burgess et al., 2019), and the choice of flow radiation factor is constrained by the seismic data that show the shape of the lobes.

4 Fan lobe spatial distribution patterns

Fan lobes in $Es4^1$ strata are picked and interpreted from seismic data based on their geometry and reflector termination patterns. Proximal fan lobes display wedge-like geometries with up-dip onlap and down-dip downlap (Fig 4a), whereas distal lobes more typically have a lenticular geometry with downlap onto the underlying strata or unresolved pinchouts (Fig 4b). Channels are featured by small scale concave geometry (“v” shape) in seismic section (Fig 4e, 4f). There are 8 fan lobes mapped in stage 1 (Fig 4c) and 12 fan lobes in stage 2 (Fig 4d).

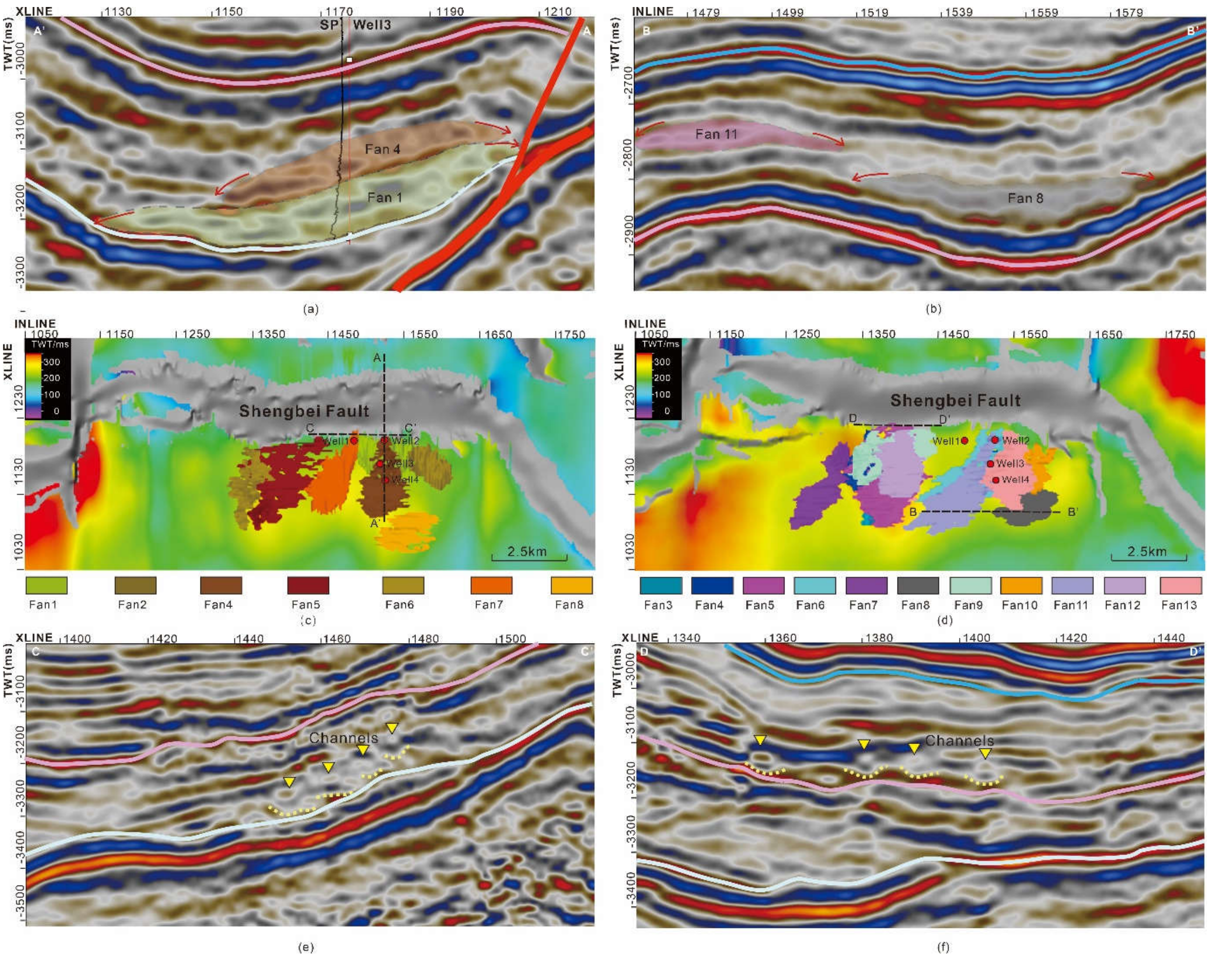

Figure 4: Fan maps in stage one and stage two interpreted from seismic and well logs. (a) fan lobes interpreted from along dip seismic profile and seismic-well tie, showing wedge-like shape (b) fan lobes interpreted form along strike seismic profile showing lenticular geometry with two ends of its top reflector onlap onto the underlying strata. (c) fan map of stage one. (d) fan map of stage two. (e) (f) Channels interpreted from along strike seismic section in stage one and stage two respectively, exhibiting concave geometry ("v" shape).

Fan maps show more confinement in Stage 2 lobes, whereas Stage 1 lobes are more dispersive. Along-strike variations in displacement rate of the Shengbei fault (Fig 5) suggest the fault probably initially comprised multiple unlinked fault segments during early syn-rift (Cowie et al 2000). This suggests increasing subsidence from synrift stage one to synrift stage two (Fig 5a). Additionally, growth folds in low displacement rate zones (Fig 5 d, e) also indicate initially separated fault segments and subsequent fault linkage (Schlische 1995; Gupta et al., 1999; Gawthorpe et al., 2000). During early synrift, the unbreached transfer zone between fault segments lacks footwall tilting to divert antecedent drainage networks and can therefore serve as an important sediment input route for turbidity flows into hanging wall depocenters (Gawthorpe et al., 1993, 2000).

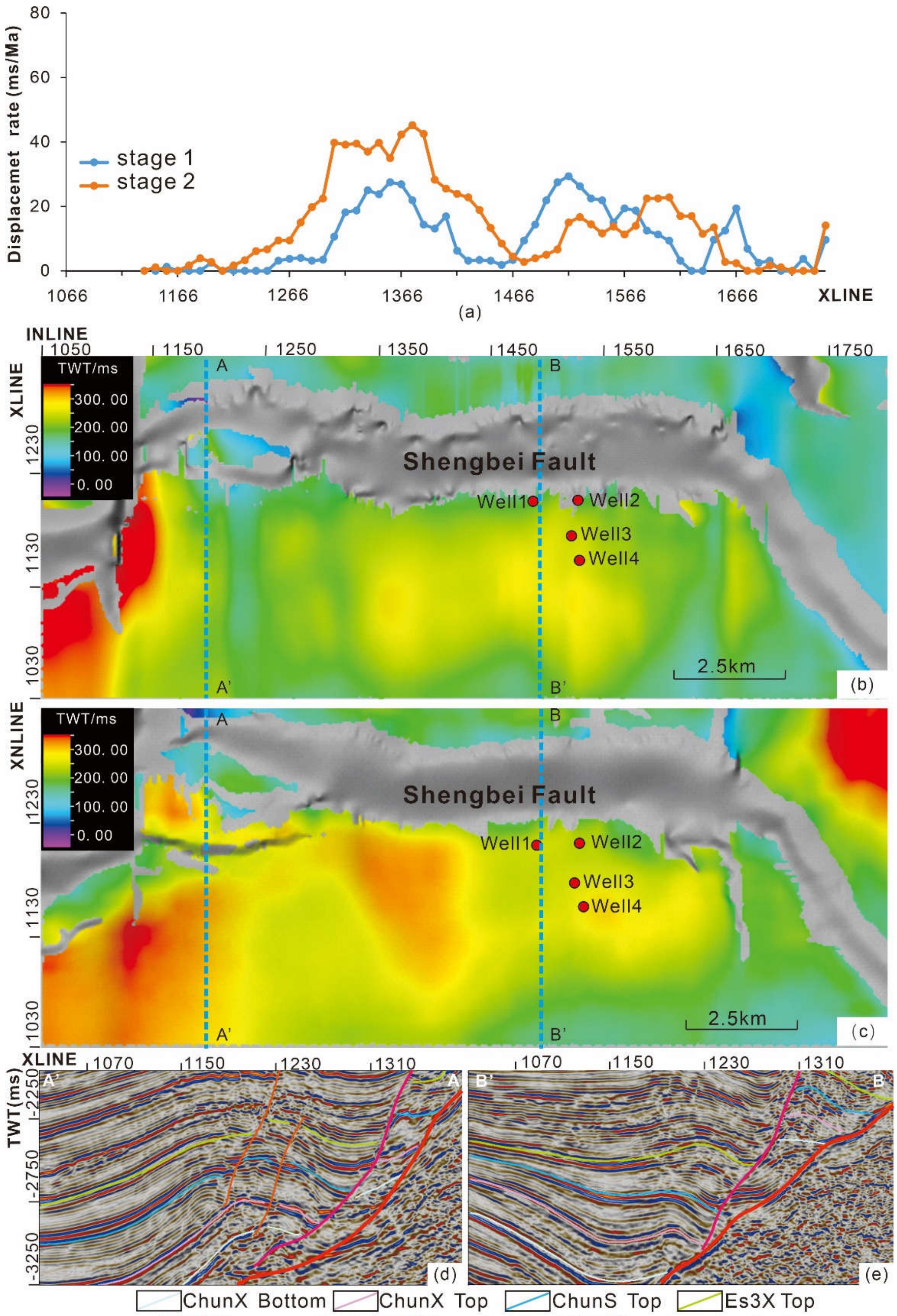

Figure 5: Variations in tectonic activity on the Shengbei Fault during stage one and stage two early syn-rift. (a) Displacement rate versus strike distance along Fault. (b) stage one thickness map plotted on the present-day structural map, yellow-orange color indicates location of hanging wall depocenters adjacent to Shengbei fault in stage one (c) thickness map of stage two plotted on the present-day structural map, yellow-orange color indicates location of hanging wall depocenter adjacent to Shengbei fault in stage two, (d)(e) seismic sections throughlow displacement rate areas showing growth fold features.

5 Reference Lobyte-3D model run

A Lobyte 3D reference model was constructed aiming to reproduce key aspects of the ChunX sub-member turbidite-dominated strata. Several minor modifications are made to the original Lobyte 3D code to: (1) model multiple fan deposition with varied sediment input volume supplied from different source point coordinates, and also to (2) model spatially variable subsidence rates. These modifications allow the model to better represent complex turbidity fan deposition in a steep-slope half-graben margin in a lacustrine basin as observed in the study area.

5.1 Input data of best-fit reference model

This model uses a 190 by 190 grid with individual grid cells of 100m by 100m. Parameter values used in the reference model were summarized in table 1.

Table 1: Major input data used in reference model and their description

Input Category	Input data	Reference value	Description
Model dimension	model grid	190*190	Grid x,y dimension
	cell size	0.1*0.1	Grid cell x,y size (km)
	time step	0.001	Interval between turbidity current events (My)
Sediment supply	d_{50}	0.00025	median grain diameter(m) (medium/fine sand)
	ρ_g	2660	Grain density(kg/m^3) in gravity flow typically quartz/feldspar
	Number of fans	8	total number of fans modelled
	Number of flow events of each fan	10 ~ 47	number of flow events comprises individual fan deposition
	Vmax	4.2 ~18.5	Maximum sediment volume(km^3) in individual gravity flow event during model run
	Vmin	1.4 ~10.5	Minimum sediment volume(km^3) in individual gravity flow during model run
	sediment supply oscillation period	25	Representing sediment supply oscillation frequency
Tectonic and topographic map	initial topographic map	/	Topography of study area before deposition of $Es4^1$
	subsidence map	/	Subsidence and uplift distribution of study area during stage one of $Es4^1$
Transport and deposition	Density of ambient water ρ_w	1000	Density of ambient water (kg/m^3) for subaqueous gravity flows.
	Basal friction coefficient C_d	0.004	Darcy-Weisbach friction coefficient used for erosion calculation (Burgess, et al. 2019)
	sediment concentration C_v	0.01	Volumetric sediment concentration of subaqueous gravity flow
	Flow radiation factor FRF	1	Control whether flow dispersion in a wider or narrower and more elongate manner. (Burgess, et al. 2019)

The initial topography map is derived from interpreted seismic data (Fig 6a), and the subsidence map is generated based on thickness map of stage one (Fig 6b). Number of flow events is estimated based on the number of individual turbidity flow events identified from core photos, calibrated by the number of sandy intervals interpreted from well logs. Lobe areas are calculated from fan maps derived from seismic. For lobes without well penetration, a linear regression relation between lobe area and number of flow events is applied, based on statistics from fan lobes where well data is available, to estimate the number of flow events of each lobe (Fig 6c). Volume of sediment input required for individual flow events is calculated based on lobe area and individual turbidity event thickness.

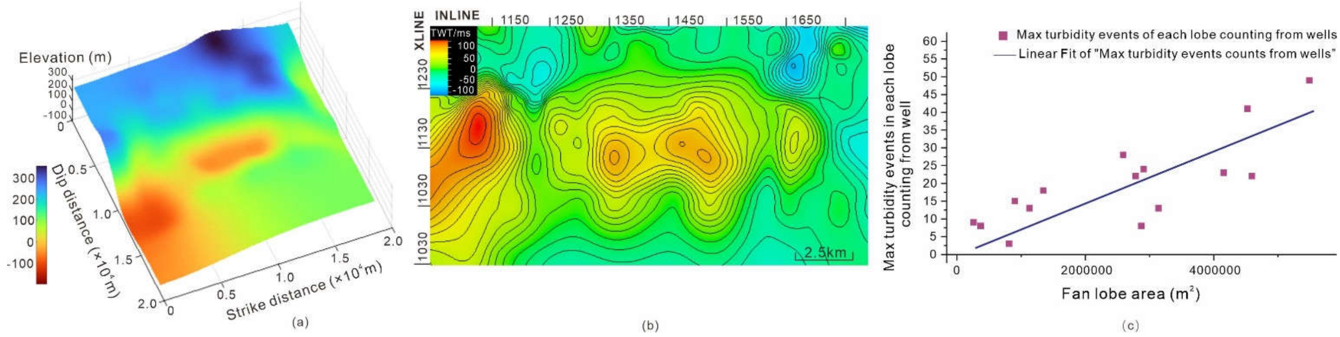

Figure 6: Some input maps and parameters for reference model run. (a) initial topography of stage one. (b) subsidence map of stage one. (c) linear regression relation between lobe area and number of flow events based on statistics from fan lobes which are penetrated by wells.

5.2 Comparison between model output and actual data

A best-fit model was produced via a trial-and-error manual calibration process using both map and vertical section data. Seismically mapped lobe location, shape and size was compared with forward modelled fan lobe planform distributions until a reasonable match was obtained (Fig 7a) including a good match with overall lobe areas (Fig. 7d). Vertical stratigraphic columns extracted from four model grid cells, located in the same relative position as the four well sites, exhibit a reasonable match with the vertical bed thickness, bed frequencies (Fig 7b) and net-gross and overall thickness (Fig 7c) interpreted from core and well logs. The three proxies exhibit an average error of 10.8% for net-gross value, 6% for stratal thickness, and 15.8% for fan area. These comparators suggest a reasonable match between the best-fit reference model and data.

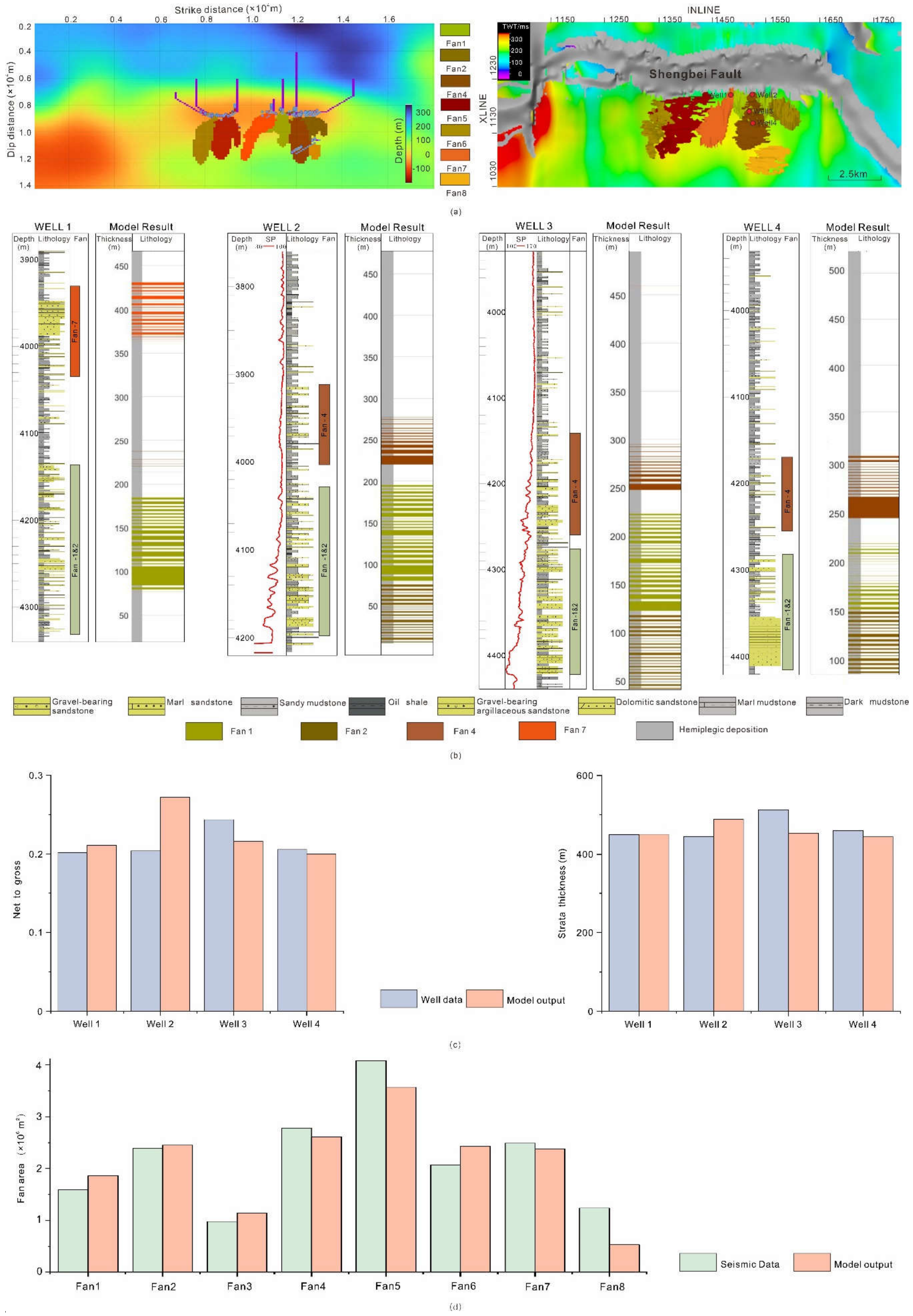

Figure 7: Comparison between model output and actual data. (a) comparison between fan maps interpreted from seismic & well log (right) and generated from Lobyte3D model run (left). (b) comparison between well logs and vertical succession extracted from Lobyte3D model output for respective well location. (c) comparison of net-to-gross (left) and overall strata thickness (right) between well data and

model output. (d) comparison of fan area between seismic interpretation and model output.

6 Sensitivity analysis of fan lobe spatial distribution to extrinsic factors

Analysis of modelled fan lobe spatial distribution is carried out to determine sensitivity to allogenic controls including fault-related subsidence, basin margin slope, sediment input volume and sediment input oscillation period. Related parameters are varied across a defined range. Fan lobe spatial distribution is quantified via consecutive flow centroid separation distance ($D_{\text{separation}}$), where greater separations suggest greater lateral movement. Mapped centroid spatial distribution (Fig 8) and frequency distribution of centroid separation distance (Fig 9) are then used to measure sensitivity of fan geometry to varying subsidence rate, margin slope, sediment input oscillation frequency and sediment input volume.

6.1 Sensitivity to subsidence rate

Non-uniform fault-related subsidence influencing paleo-topography change is a significant feature in the study area. To investigate influence of subsidence rate on lobe lateral mobility and vertical stacking we run models with the best-fit reference model inputs, except for modified subsidence rate. Three forward models are calculated with subsidence rate ranging from zero subsidence rates to 1.4 times the reference model subsidence rate. Model results show increasingly clustered flow centroids as subsidence rate increases (Fig 8 a-c, Fig 9a). This suggests fan lobe lateral movement decreases as subsidence rate increases because higher subsidence rate decreases the impact of depositional topography, and decreases the avulsion rate which is the key process creating lateral variability in the lobe strata (Bridge & Leeder 1979; Koo et al., 2016; Meek et al., 2020; Brooks et al., 2022)

6.2 Sensitivity to fault-related margin slope

To test the influence of margin slope on fan lateral mobility, we use three different slope values across a range from 0.6 to 1.4 times the reference model margin slope, with other input parameters unchanged. The results show that steeper margin slope will lead to slightly more clustered lobe deposition (Fig 8 d-f, Fig 9b) probably due to greater flow velocity creating deeper and more confined channels (Yu et al., 2013). Flow centroid positions show that fan lobes deposition always starts at the slope-to-basin-floor break of slope (Fig 8) irrespective of variation in basin-margin slope (Fig 8 d-f), which indicates that break of slope is a more important control on the location and deposition of fan lobe strata than the up-dip slope gradient. The abrupt slope gradient decrease at break of slope can decelerate the flows, triggering dispersive deposition.

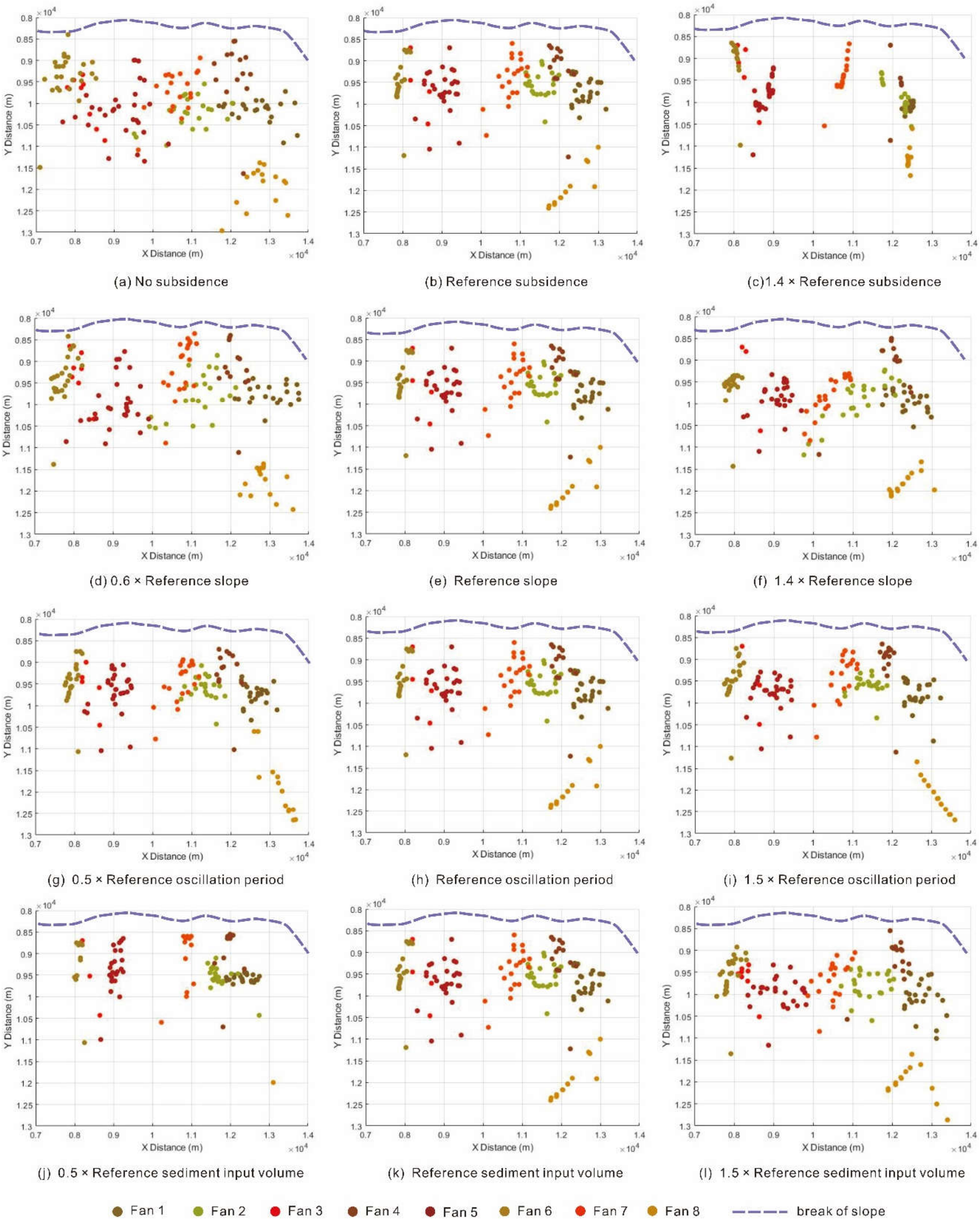

Figure 8: Maps of flow bed centroid map view spatial distribution. (a-c) Varying subsidence rate from no subsidence to 1.3 times the reference subsidence, showing more clustered stacking of fan lobes as subsidence increases (d-f) Varying slope from 0.6 to1.4 times the reference slope, showing a little more convergent stacking pattern of fan lobes as margin slope increases. (g-i) Varying sediment input oscillation period from 0.5 to 1.5 times the reference oscillation period, showing no significant fan lobe distribution difference. (j-l) Varying sediment input volume, showing more dispersive stacking as supply volume increases.

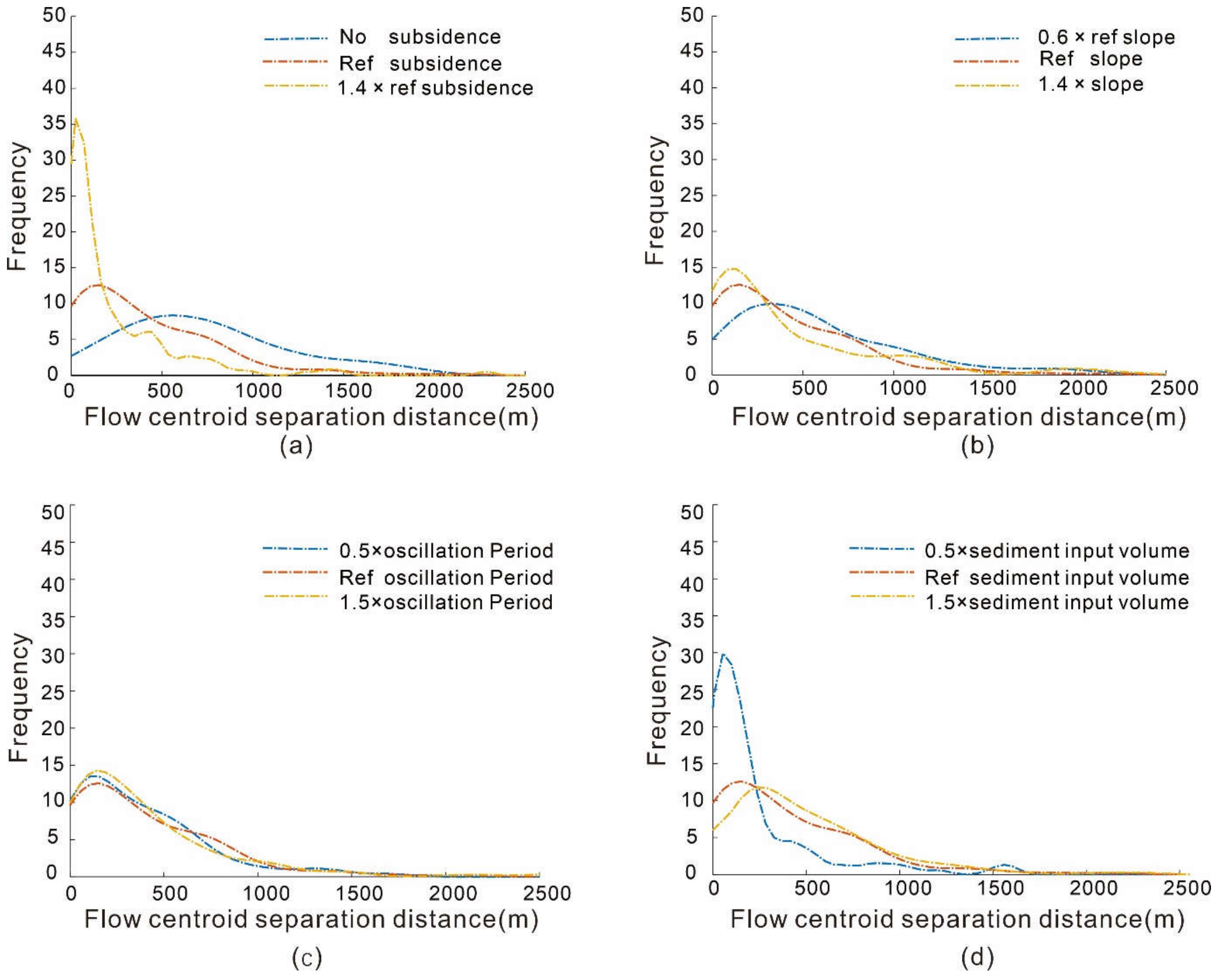

Figure 9: Frequency distribution plots of flow centroid separation distance under external influences (a) lower subsidence produces more dispersive flow bed distribution, greater subsidence lowers the mean centroid separation and results in more clustered distribution , (b)margin slope is a minor control, greater margin slope produces slightly more clustered distribution, (c) sediment oscillation period have no obvious influence on lobe spatial distribution (d) greater sediment input volume produces more dispersive flow bed distribution.

6.3 Sensitivity to sediment input oscillation period

Sediment input oscillation period reflects the frequency at which flow volumes fluctuate between maximum and minimum representing changes in climatic and tectonic forcing of flow volumes. In this test, we used three different oscillation period ranging from 0.5 to 1.5 times the reference oscillation period. The results show that no flow bed distribution difference is observed as sediment input oscillation period varied (Fig 8 g-i, Fig 9c), indicating that sediment input oscillation frequency doesn't have significant influence on fan lobe lateral movement.

6.4 Sensitivity to sediment input volume

Variable sediment input volume is a key allogenic control on submarine fan evolution (Koo et al., 2016; Meek et al., 2020; Ferguson et al.,2020). Sediment input volume is varied from 0.5 to 1.5 times the best-fit reference input volume. The results suggest that flow beds are less clustered as sediment input volume increases, exhibiting a relatively strong sensitivity (Fig 8 j-l Fig 9d) probably due to greater supply input infilling the topographic low relief more, smoothing out the basin floor relief and reducing the confinements of topography on turbidity flow. This may further imply that turbidity fan lobes formed under humid climate where higher sediment influx is usually triggered by greater precipitation and water discharge can exhibit wider and more dispersive spatial distribution than that formed under more arid climate. Comparing with the result of sediment input oscillation period, it also indicates that changing supply oscillation period (Fig 9c) has no significant effect on fan lobe morphology or stacking, but changing the magnitude of supply input volume does have some systemic effect.

6.5 Comparison with submarine fan lobes

Submarine and lacustrine environments may both be controlled by extrinsic factors such as asymmetric subsidence, slope and sediment supply controlling fan lobe distribution and stacking patterns. For example, previous studies indicate that submarine fan lobes formed on tectonically active basin margins (Brooks et al., 2022) commonly feature a fixed, aggradational base-of-slope position, whereas those formed in tectonically quiescent basins expand and contracting with more variable stacking behaviour (Brooks et al., 2018). Similarly, Koo et al. (2016) showed that base-of-slope high-supply submarine fans tend to be more extensive than the more localized fans with relatively fixed slope channels that develop in accommodation-dominated settings (Koo et al., 2016). These submarine fan patterns are in line with these modelling results discussed above. Previous studies also found that stacking behaviour of deep-water submarine lobe complexes can be linked to the coeval shelf-edge delta's stacking patterns and overall shelf-edge trajectory (Koo et al., 2016), but no shelf-edge delta is observed in the smaller-scale lacustrine basin in this study.

7 Reservoir presence prediction

Because the best-fit model (Fig 7a) is probably not a unique best fit, predictive power of such a single calibrated reference model is likely to be limited. Therefore, a multiple scenario approach which varies parameters within their respective uncertainty range to generate a series of best-fit models (Burgess et al., 2006; Agrawal, D., 2015; Gervais et al., 2017) is adopted. to better understand the impact of parameter uncertainty on the model output, and to enhance the reservoir presence predictive power of the modelling.

Four sets of models are calculated, each containing 12 best-fit scenarios with 8 non-fit scenarios being discarded in each set (Fig 10 a). Respective model sets investigate fault-related subsidence, fault-related margin slope, sediment input oscillation period and sediment input volume and models from each set are used to calculate a conditional probability map that is also a reservoir presence map (Burgess et al., 2006). All other parameters have the best-fit model values.

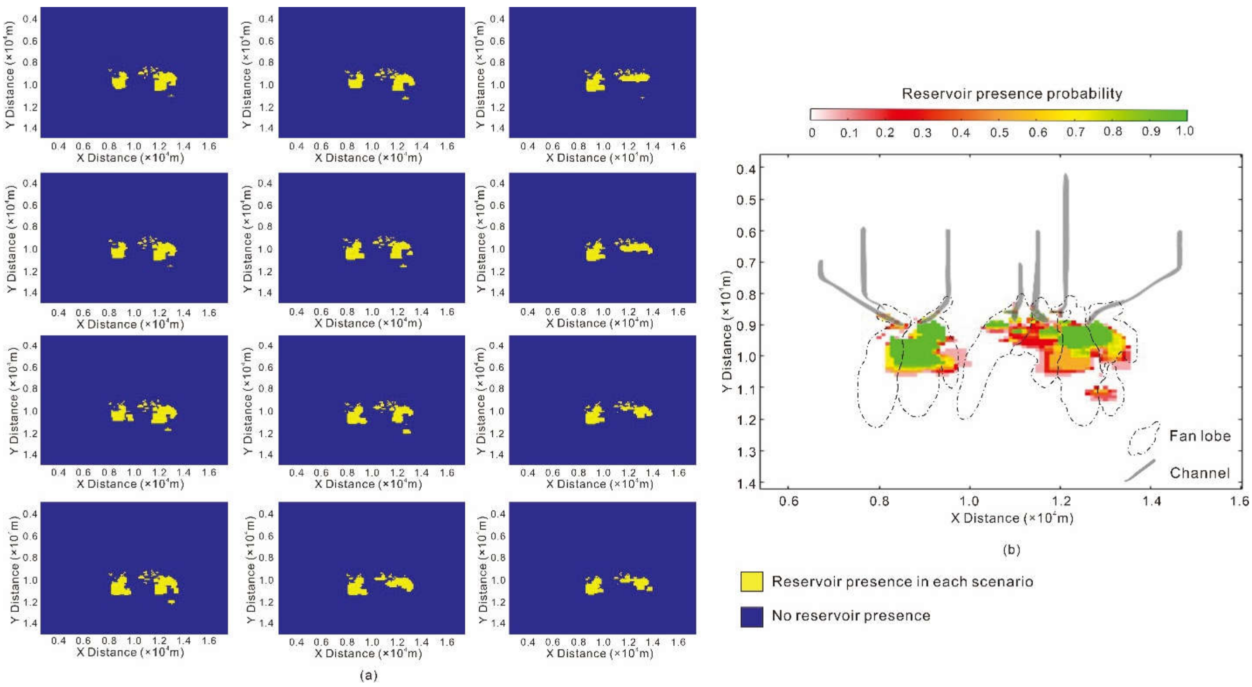

Figure 10: Multiple scenario approach and conditional probability map. (a) 12 scenarios of reservoir presence in study area generated by varying subsidence rate within its uncertainty range. (b) a reservoir presence probability map exclusively considering the subsidence rate parameter is produced by combining the 12 scenarios together, where green area indicates high likelihood for reservoir presence whereas red indicates low likelihood.

Conditional probability maps are defined by the following criteria: (1) the thickness of an individual turbidite bed is greater than 5m, (2) reservoir occurred in the middle 1/3 section of an individual flow bed (which represents the optimal grain size). The conditional probability map is then calculated such that

$$P_{x,y} = \frac{\sum_{1}^{n_s} C_{x,y}}{n_s}$$

where P is the conditional probability at any x,y model grid cell, n_s is the total number of model runs in the set being used to calculate the map, and C is the result of the criteria test at each x, y point on the model grid, 1 if the criteria are met, and 0 otherwise. The conditional probability map is then presented as a reservoir presence probability map with colour coding such that high probability of reservoir, when most models meet the criteria at a grid point, is green to yellow, low probability is red, and zero probability is white (Fig 10b).

Following this procedure four reservoir presence probability maps are calculated and plotted from the sensitivity analysis model sets (Fig 11). The maps are similar overall but do exhibit some important variability. Areas of reservoir presence probability greater than 80% compose 2.9% (Fig 11a), 3.3% (Fig 11b), 3.4% (Fig 11c), 3.6% (Fig 11d) of the entire fan deposition area. Predicted best reservoir is more laterally extensive in the subsidence model sets (Fig 11a) and more elongated down-dip in the margin slope, sediment input oscillation period and sediment input volume model sets (Fig 11B, C&D), indicating that fan lobe lateral migration is most sensitive to subsidence rate.

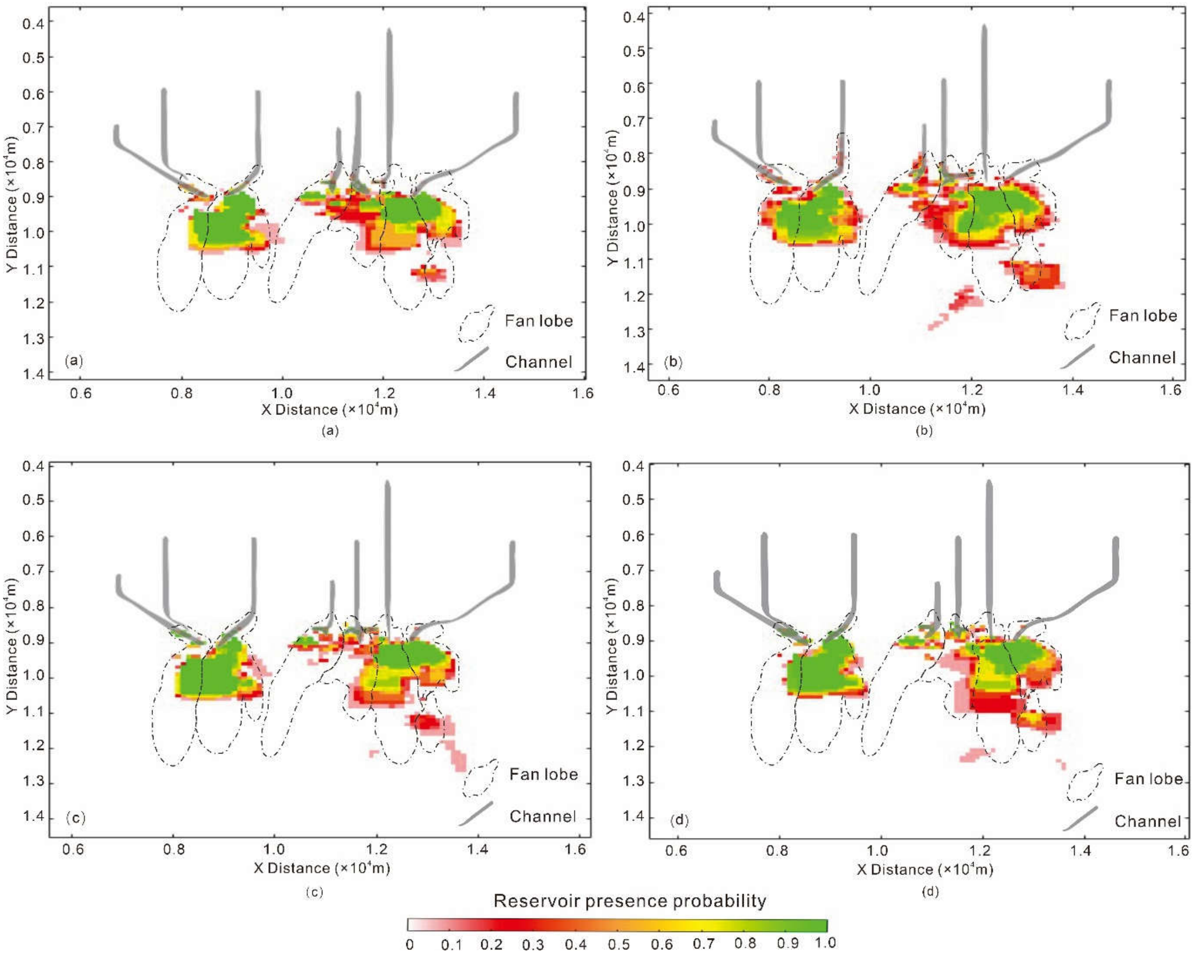

Figure 11: Reservoir presence probability maps produced by considering (a) subsidence rate, (b) margin slope, (c) sediment oscillation period and (d) sediment input volume separately, showing that, despite their resemblance, the reservoir presence areas of map (a) and (b) are more laterally extended whereas that of map (c) and (d) are elongated more in the down-dip direction

Combining all 48 model scenario outputs into one reservoir presence probability map (Fig 12) highlights locations where the presence of good reservoir is relatively insensitive to the uncertainty in the subsidence rate, sediment input oscillation period, margin slope, and sediment input volume. Best reservoir mainly occurs in the middle fan area with some more scattered sweet spots in feeder channels and inner fan area.

Sweet spot area located at basin floor down-dip of the break of slope indicates bypass dominated inner to middle fan deposition. It is more laterally dispersive covering a greater area, and the reservoir presence probability decreases toward outer fringe due to the lack of thick beds. Whereas reservoir located at up-dip of the slope break is retrogradational backstep dominated feeder channels deposition which is formed by channel backfilling and lobe retrogradation (Hamilton et al., 2013; Haas et al., 2016; Meek et al., 2020, Ferguson et l.,2020). It is more laterally confined and scattered at the lower slope. Outer fan areas show lower reservoir presence probability, simply due to absence of thick beds and coarse grains. Therefore, in the fault-controlled basin margin, besides the middle fan area on basin floor, some lower slope feeder channel could also be a possible sweet spot location.

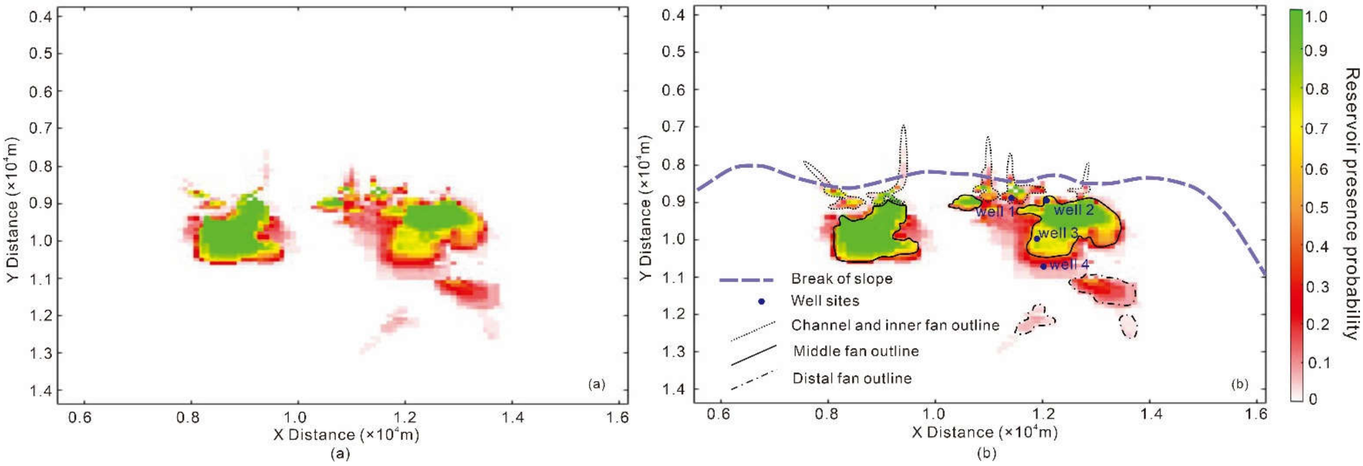

Figure 12: Final reservoir presence probability map by combining all the 48 scenarios outputs of the four external factors, showing that middle fan area and part of feeding channels in inner fan area are more greenish which means these areas are most likely for good quality reservoir to occur in study area.

8 Conclusion

1. During the early syn-rift stage, the Shengbei fault comprised multiple smaller fault segments with displacement rates decreasing from the segment centres towards segment tips. The unbreached transfer zone between two fault segments served as the sediment influx pathway for turbidity flow to transport into hanging wall depocenters.

2. External controls exert systematic impact on the spatial distribution of both larger-scale fans and smaller-scale flow beds on basin floor. The tectonic setting of the early syn-rift basin margin controlled location of sediment input points through transfer zones between two fault segments, and local subsidence, which further controls the locus and aggradation of larger-scale fans. The non-uniform fault-related subsidence and sediment input volume can also modify basin floor topography significantly, either creating or smoothing out basin-floor relief, which in return impact the interaction between turbidity flow and depositional topography that influences the loci of erosion and deposition of subsequent flows, controlling smaller-scale flow bed geometry and stacking.

3. Fault-related subsidence is a significant control. Greater fault-related subsidence produces more laterally confined fan lobe distribution. Fault-related basin-margin slope gradient is a relatively minor control producing only slightly more clustered flow bed deposition. Higher sediment input volume produces more dispersive fan lobe distribution, but changing supply oscillation period has no systematic effect on fan lobe morphology or stacking.

4. Despite demonstrated allogenic control, in all the included model runs, location of fan lobe deposition is always determined by the position of the slope-to-basin-floor break of slope which is a key control on the location of fan lobe strata. This is a consequence of model assumptions of flow velocity being a function topographic gradient and a simple velocity threshold for dispersive deposition. If these assumptions are realistic, this result is perhaps predictive for real deep-water depositional systems.

5. Multiple scenarios reservoir presence probability map suggests that some bypass-dominated middle-to-inner fan areas, and sections of the retrogradationally-filling lobe feeder channels have best reservoir presence probability.

Acknowledgements

This research was funded by the National Natural Science Foundation of China (Grant No. U19B2006), the CSC funding (China Scholarship Council, No.202106450029), the National Natural Science Foundation of China (Grant No. 42102187), the Natural Science Foundation of Chongqing (No. CSTB2022NSCQ-MSX118). We also would like to thank the data from Shengli Oil Field, China Petroleum & Chemical Corporation (SINOPEC) and the license of Petrel software from Schlumberger to support this research.

Conflict of interest

There is no conflict of interest in the preparation or publication of this work.

Reference

Alghuraybi, A., Bell, E. R., & Jackson, C. (2022). The geometric and temporal evolution of fault-related folds constrain normal fault growth patterns, Barents sea, offshore Norway. B*asin Research*, 34(2), 618-639. https://doi.org/10.1111/bre.12633

Allen, M. B., Macdonald, D., Xun, Z., Vincent, S. J., & Brouet-Menzies, C. (1997). Early cenozoic two-phase extension and late Cenozoic thermal subsidence and inversion of the Bohai Basin, Northern China. *Marine & Petroleum Geology,* 14(7), 951-972. https://doi.org/10.1016/S0264-8172(97)00027-5

Agrawal, D., Dwivedi, S., Barrois, A., Koeck, C. H., & Aillud, G. (2015). Impact of Environmental Parameters on Forward Stratigraphic Modelling from Uncertainty Analysis; Lower Cretaceous, Abu Dhabi. SPE Reservoir Characterisation & Simulation Conference & Exhibition Held in Abu Dhabi. DOI: 10.2118/175683-MS

Barry, J., & Liu, X. (1998). Summary of the AAPG research symposium on lacustrine basin exploration in china and southeast Asia. *AAPG Bulletin*, 82(7), 1300-1307. DOI: 10.1306/1d9bca57-172d-11d7-8645000102c1865d

Brooks, L.H., Ito, M., Zuchuat, V., Peakall, J. & Hodgson, M., D. (2022). Channel-lobe transition zone development in tectonically active settings: Implications for hybrid bed development. *The depositional Record,* 8 (2), 829-868. https://doi.org/10.1002/dep2.180

Brooks, H.L., Hodgson, D.M., Brunt, R.L., Peakall, J., Hofstra, M. & Flint, S.S. (2018). Deep water channel-lobe transition zone dynamics: processes and depositional architecture, an example from the Karoo Basin, South Africa. Geological Society of America Bulletin, 130, 1723–1746. https://doi.org/10.1130/ B31714.1

Burgess, P. M., Lammers H., Oosterhout C., & Granjeon D. (2006); Multivariate sequence stratigraphy: Tackling complexity and uncertainty with stratigraphic forward modeling, multiple scenarios, and conditional frequency maps. *AAPG Bulletin*, 90 (12): 1883–1901. https://doi.org/10.1306/06260605081

Burgess, P.M., Masiero, I., Toby, S.C., & Duller, R.A. (2019) A big fan of signals? Exploring autogenic and allogenic process and product in a numerical stratigraphic forward model of submarine-fan development. *Journal of Sedimentary Research*, 89, 1–12. https://doi.org/10.2110/jsr.2019.3

Bridge, J. S., & Leeder, M. R. (1979). A simulation model of alluvial stratigraphy. Sedimentology, 26(5). 617-644. https://doi.org/10.1111/j.1365-3091.1979.tb00935.x

Cecil, C.B. (2003). The concept of autocyclic and allocyclic controls on sedimentation and stratigraphy, emphasising the climatic variable. In Cecil, C.B. and Edgar, N.T. (Eds.) Climate Controls on Stratigraphy. *SEPM Special Publications,* 77, 13–20. https://doi.org/10.2110/pec.03.77.0013

Cowie, P. A., Gupta, S., & Dawers, N. H. (2000). Implications of fault array evolution for synrift depocentre development: insights from a numerical fault growth model. *Basin Research*. 12, 241–261. https://doi.org/10.1111/j.1365-2117.2000.00126.x

Cullis, S., Colombera, L., Patacci, M., & Mccaffrey, W. D. (2018). Hierarchical classifications of the sedimentary architecture of deep-marine depositional systems. *Earth-Science Reviews*, 179, 38-71. https://doi.org/10.1016/j.earscirev.2018.01.016

Dawers, N. H., & Anders, M. H. (1995). Displacement-length scaling and fault linkage. *Journal of Structural Geology*, 17(5), 607-614. https://doi.org/10.1016/0191-8141(94)00091-D

Deutsch, C. V., (2002), Geostatistical reservoir modeling (applied geostatistics): Oxford, Oxford University Press, 384 p.

Feng, Y., Li, S., & Lu, Y. (2013). Sequence stratigraphy and architectural variability in late eocene lacustrine strata of the Dongying depression, Bohai Bay Basin, Eastern China. *Sedimentary Geology*, 295(8), 1-26. https://doi.org/10.1016/j.sedgeo.2013.07.004

Ferguson, R., Kane, I. A., Eggenhuisen, T.J., Pohl, F., Tilson, M., Spychala, T.Y. & Brunt, L.R. (2020). Entangled external and internal controls on submarine fan evolution: an experimental perspective. *The Depositional Record*, 6:605–624. DOI: 10.1002/dep2.109

Gawthorpe, R. L., & Hurst, J. M. (1993). Transfer zones in extensional basins: their structural style and influence on drainage development and stratigraphy, *Journal of the Geological Society*, London, Vol. 150, 1993, pp. 1137-1152,

Gawthorpe, R. L., & Leeder, M. R. (2000). Tectono-sedimentary evolution of active extensional basins, 12,195–218. *Basin Research*. https://doi.org/10.1111/j.1365-2117.2000.00121.x

Gervais V., Ducros, & M., Granjeon, D. (2018). Probability maps of reservoir presence and sensitivity analysis in stratigraphic forward modeling. *AAPG bulletin*, 102(4), 613-628. http://DOI:10.1306/0913171611517242

Groenenberg, R. M., Hodgson, D. M., Prelat, A., Luthi, S. M., & Flint, S. S. (2000). Flow–deposit interaction in submarine lobes: insights from outcrop observations and realizations of a process-based numerical model. *Journal of Sedimentary Research*, 80(3), 252-267. https://DOI: 10.2110/jsr.2010.028.

Gupta, S., Underhill, R. J., Sharp, R. I. & Gawthorpe, R. L. (1999). Role of fault interactions in controlling synrift sediment dispersal patterns: Miocene, Abu Alaqa group, Suez rift, Sinai, Egypt. *Basin Research*, 11(2). https://doi.org/10.1046/j.1365-2117.1999.00300.x

Haas, T. D., Wilco, V., Braat, L., Kleinhans, M. G., & Mohrig, D. (2016). Autogenic avulsion, channelization and backfilling dynamics of debris-flow fans. *Sedimentology*. (2016) 63, 1596–1619, doi : 10.1111/sed.12275.

Hamilton, P. B., Strom, K., & Hoyal, D. (2013). Autogenic incision-backfilling cycles and lobe formation during the growth of alluvial fans with supercritical distributaries. *Sedimentology*, 60(6), 1498-1525. doi: 10.1111/sed.12046

Jiang, Z., Liu, H., Zhang, S., Xin, S., & Jiang, Z. (2010). Sedimentary characteristics of large-scale lacustrine beach-bars and their formation in the Eocene Boxing sag of Bohai Bay Basin, East China.

Sedimentology. 58,1087–1112, https://doi.org/10.1111/j.1365-3091.2010.01196.x

Jin, Q., Wang, R., Zhu, G., Yi, Z., & Rong, Q. (2005). The lacustrine Liangjialou fan in the Dongying depression, Eastern China: deep‐water reservoir sandstones in a non‐marine rift basin. *Journal of Petroleum Geology*, 28(4) :397 – 412, DOI:10.1111/j.1747545. 2005. tb00090.x

Kneller, B. (1995). Beyond the turbidite paradigm: physical models for deposition of turbidites and their implications for reservoir prediction. Characterization of Deep Marine Clastic Systems, 94(1), 31-49, *Geological Society, London, Special Publications*, https://doi.org/10.1144/GSL.SP.1995.094.01.04

Knudson, K.P. & Hendy, I.L. (2009) Climatic influences on sediment deposition and turbidite frequency in the Nitinat Fan, British Columbia. *Marine Geology*, 262, 29–38. https://doi.org/10.1016/j. margeo.2009.03.002

Koo, M.W., Olariu, C., Steel J.R., Olariu, I.M., Carvajal, R.C., & Kim, W. (2016). Coupling between shelf-edge architecture and submarine-fan growth style in a supply-dominated margin. *Journal of Sedimentary Research*, 86 (6): 613–628. doi: https://doi.org/10.2110/jsr.2016.42

Li, J., Liu, Z., Liu, J., Liang, C., Liu, H., Huang L., Qain L., Lu, K., & Liu, K. (2021). Transformation of sediment delivery and dispersal patterns controlled by relay-ramp evolution along the boundary fault of a lacustrine rift: the Eocene Shahejie Formation, Dongying sag, Bohai Bay Basin, NE China. *Marine and Petroleum Geology*, 128. https://doi.org/10.1016/j.marpetgeo.2021.105044

Liu, M, & Xiong, C. (2021). Diagenesis and reservoir quality of deep-lacustrine sandy-debris-flow tight sandstones in upper Triassic Yanchang Formation, Ordos Basin, China: implications for reservoir heterogeneity and hydrocarbon accumulation. *Journal of Petroleum Science and Engineering*, 202,1-18, https://doi.org/10.1016/j.petrol.2021.108548.

Luan, G., Azmy, K., Dong, C., Lin, C., Ren, L., & Shi, C. (2022). Carbonate cements in eocene turbidite sandstones, Dongying depression, Bohai Bay Basin: origin, distribution, and effect on reservoir properties. *AAPG Bulletin*, 106(1):209-240, DOI: 10.1306/07202120012

Mackie, W. A., Stevenson J. C. & Burgess, M. P., Complexity is simple: stratigraphic development and organisation within a reduced-complexity 2d forward model. (in review)

Ma, P., Lin, C., Ren, L., Jahren, J., Jahren,J., Dong, D., Yu, G., Ma, C., Wang, D., Liu, L.,& Hellevang, H. (2021). Linkage and growth of the independent and coherent faults: insight into the effect of relay ramps on sedimentation patterns in the northern bonan sag, bohai bay basin. *Marine and Petroleum Geology*, 127, 104985. https://doi.org/10.1016/j.marpetgeo.2021.104985

Meek, S. R., Carrapa, B., & Decelles, P. G. (2020). Recognizing allogenic controls on the stratigraphic architecture of ancient alluvial fans in the Western US. *Frontiers in Earth Science*, 8 (215), 1- 20. https://doi: 10.3389/feart.2020.00215.

Nelson, C.H., Escutia, C., Goldfinger, C., Karabanov, E., Gutierrez, J. & De Batist, M. (2009). Exernal controls on modern clastic turbidite systems: three case studies. In Kneller, B., Martinsen, O.J. and McCaffrey, B. (Eds.) External Controls on Deep-Water Depositional Systems. *SEPM Special Publications*, 92, 57–76. https://doi.org/10.2110/sepmsp.092.057

Nixon, C. W., Mcneill, L. C., Bull, J. M., Bell, R. E., Gawthorpe, R. L., Henstock, T. J., Christodoulou, D., Ford, M., Taylor, B., Sakellariou, D., Ferentinos, G., Papatheodorou, G., Leeder, R.M., Collier, R. E., Goodliffe, M. A., Sachpazi, M., & Kranis, H. (2016). Rapid spatiotemporal variations in rift structure during development of the corinth rift, central Greece. *Tectonics*, 35(5). 1225-1247, https://doi.org/10.1002/2015TC004026

Normark, W.R., Piper, D.J.W., & Sliter, R. (2006) Sea-level and tectonic control of middle to late Pleistocene turbidite systems in Santa Monica Basin, offshore California. *Sedimentology*, 54, 867–897. https://doi.org/10.1111/j.1365-3091.2006.00797.x

Prélat A., Hodgson, D. M., & Flint, S. S. (2010). Evolution, architecture and hierarchy of distributary deep-water deposits: a high-resolution outcrop investigation from the permian karoo basin, south africa. *Sedimentology*, 56(7), 2132-2154. doi :10.1111/j.1365309.2009.01073.x

Prélat, A., Covault, J.A., Hodgson, D.M., Fildani, A. & Flint, S.S. (2010). Intrinsic controls on the range of volumes, morphologies, and dimensions of submarine lobes. S*edimentary Geology*, 232(1–2), 66-76. doi : 10.1016/j.sedgeo.2010.09.010

Schlische, R. W. (1995). Geometry and origin of fault-related folds in extensional settings. *AAPG Bulletin*. 79 (11), 1661–1678. https://doi.org/10.1306/7834DE4A-1721-11D7-8645000102C1865D

Sprague, A.R.G., Garfield, T.R., Goulding, F.J., Beaubouef, R.T., Sullivan, M.D., Rossen,C., Campion, K.M., Sickafoose, D.K., Abreu, V., Schellpeper, M. E., Jensen, G.N., Jennette, D.C., Pirmez, C., Dixon, B.T., Ying, D., Ardill, J., Mohrig, D.C., Porter, M.L., Farrell, M.E., & Mellere, D. (2005). Integrated slope channel depositional models: the key to successful prediction of reservoir presence and quality in offshore West Africa. *CIPM Conference*. Veracruz, Mexico, 5 ,1-13.

Starek, D., & Fuksi, T. (2017). Distal turbidite fan/lobe succession of the late oligocene zuberec fm. – architecture and hierarchy (Central Western Carpathians, Orava–Podhale Basin). *Open Geoscience*s, 9(1), 385-406. https://doi.org/10.1515/geo-2017-0030

Tao, Z., He, Z., Alves, T. M., Guo, X., Gao, J., & He, S., et al. (2022). Structural inheritance and its control on overpressure preservation in mature sedimentary basins (dongying depression, bohai bay basin, china). *Marine and Petroleum Geology*, 137,1-14. https://doi.org/10.1016/j.marpetgeo.2021.105504

Wang, Y., Straub, K.M. & Hajek, E.A. (2011) Scale-dependent compensational stacking: An estimate of autogenic time scales in channelized sedimentary deposits. *Geology*, 39, 811–814. https://doi.org/10.1130/G32068.1

Wang, X., He, S., Wei, A., Liu, Q., & Liu, C. (2016). Typical disequilibrium compaction caused overpressure of paleocene dongying formation in northwest Liaodongwan depression, Bohai Bay Basin, China. *Journal of Petroleum Science & Engineering*, 726-734. https://doi.org/10.1016/j.petrol.2016.09.014

Weimer, P., Slatt, M. R., Dromgoole P., Bowman, M., &Leonard, A. (2000). Developing and managing turbidite reservoirs: case histories and experiences: results of the 1998 EAGE/AAPG Research Conference. *AAPG Bulletin*, 84(4), 453-465. https://doi.org/10.1306/C9EBCE0F-1735-11D7-8645000102C1865D

Wendebourg, J., (2002), Uncertainty of petroleum generation using methods of experimental design and response surface modeling: Application to the Gippsland Basin, Australia, *AAPG Bulletin*, 7:295-307. DOI: 10.1306/A967517E-1738-11D7-8645000102C1865D

Yang, T., Cao, Y., Liu, K., Wang, Y., Zavala, C., Friis, H., Song M., Yuan, G., Liang C., Xi, k., & Wang, j. (2019). Genesis and depositional model of subaqueous sediment gravity-flow deposits in a lacustrine rift basin as exemplified by the Eocene Shahejie Formation in The Jiyang Depression, Eastern China. *Marine and petroleum geology*. https://doi.org/10.1016/j.marpetgeo.2018.12.033

Zhang, L., Liu, Q., Zhu, R., Zheng, L., & Lu, X. (2009). Source rocks in Mesozoic–Cenozoic continental rift basins, east china: a case from Dongying depression, Bohai Bay Basin. *Organic Geochemistry*, 40(2), 229-242. https://doi.org/10.1016/j.orggeochem.2008.10.013

Zhao, X., Zhou, L., Xiugang, P. U., Jin, F., Han, W., Xiao, D., Chen S., Shi, Z., Zhang, W., & Yang, F. (2018). Geological characteristics of shale rock system and shale oil exploration breakthrough in a lacustrine basin: a case study from the paleogene 1st sub-member of kong 2 member in Cangdong sag, Bohai Bay Basin, China. *Petroleum Exploration and Development* (3), 377-388. DOI:10.11698/PED.2018.03.01